Modern Physics Letters B, Vol. 23, No. 10 (2009) 1359–1366

World Scientific
www.worldscientific.com

LOW-FIELD ELECTRON TRANSPORT PROPERTIES IN ZINCBLENDE AND WURTZITE GaN STRUCTURES USING AN ITERATION MODEL FOR SOLVING BOLTZMANN EQUATION

H. ARABSHAHI*,‡ and A. A. MOWLAVI†

*Department of Physics, Ferdowsi University of Mashhad,
P.O. Box 91775-1436, Mashhad, Iran
†Department of Physics, Tarbiat Moallem University of Sabzevar, Iran
‡arabshahi@um.ac.ir

Received 2 June 2008
Revised 20 July 2008

An iteration calculation has been carried out to study electron transport properties in zincblende and wurtzite GaN materials. The two-mode nature of the polar optic phonons is considered jointly with deformation potential acoustic, piezoelectric, ionized impurity scattering. Band non-parabolicity, admixture of p functions, arbitrary degeneracy of the electron distribution, and the screening effects of free carriers on the scattering probabilities are incorporated. Electron drift mobility in both zincblende and wurtzite GaN crystal structures are calculated for different temperature and doping dependencies. It is found that the electron mobility decreases monotonically as the temperature increases from 100 K to 600 K. The low temperature value of electron mobilty increases significantly with increasing doping concentration. The agreement of iterative results with the available experimental data is found to be satisfactory.

Keywords: Iterative; deformation potential; piezoelectric; nonparabolicity; mobility.

1. Introduction

Gallium nitride has long been considered a promising material for electronic and optoelectronic device applications.[1–4] The wide and direct energy gap, large breakdown field, high thermal conductivity, and favorable electron-transport characteristics, make the GaN ideally suited for high-power and high-speed applications. While initial efforts to study this material was hindered by growth difficulties, recent improvements in the material quality have made possible the realization of a number of GaN-based devices. In particular, lasers,[5] transistors and photodetectors[6] have been fabricated with these materials. These developments have fueled considerable interest in the GaN material. In order to analyze and improve the design of GaN-based devices, an understanding of the electron transport that occurs within these materials is necessary. While electron transport in bulk GaN has been extensively examined,[7–9] the sensitivity of these results to variations in the material parameters has yet to be considered.

This paper presents the iteative calculation results of electron transport in bulk GaN materials. Most of the calculations have been carried out using a non-parabolic ellipsoidal valley model to describe transport in the conduction band. However, the simpler and less computationally intensive spherical parabolic band scheme has also been applied, to test the validity of this approximation. The iterative calculations take into account the electron-lattice interaction through polar optical phonon scattering, deformation potential acoustic phonon scattering (treated as an elastic process), piezoelectric and electron–plasmon scattering. Impurity scattering due to ionized and neutral donors is also included, with the latter found to be important at low temperature due to the relatively large donor binding energy which implies considerable carrier freeze-out at low tempearure. This paper is organized as follows.

Details of the iterative model and the electron mobility calculations are presented in Sec. 2 and the results of iterative calculations carried out on GaN structures are interpreted in Sec. 3.

2. Model Details

In principle, the iterative and Monte Carlo techniques give exact numerical predictions of electron transport phenomena in bulk semiconductors.[10,11] Both of them can include the details of the microscopic electronic processes and can be extended to time-dependent phenomena. In low electric fields, the effects of scattering, which depend on the details of the distribution function, can be dealt with more conveniently by the iterative technique because it processes the whole distribution function at each step of the procedure. In contrast, the Monte Carlo method is highly susceptible to statistic fluctuations in the ensemble when the departure from equilibrium is small because of the weakness of the electric field effects.[12−14] For these reasons, we used the iterative method to determine the low field electron mobility in bulk GaN.

Rode's iterative technique provides a compact method of solution of the Boltzmann equation in the low field regime.[15−17] The Boltzmann transport equation for the distribution function $f(\mathbf{r}, \mathbf{k}, t)$ is

$$\frac{\partial f}{\partial t} + \mathbf{v} \cdot \nabla_r f + \frac{e\mathbf{F}}{\hbar} \cdot \nabla_k f = \left(\frac{\partial f}{\partial t}\right)_{\text{coll}}, \tag{1}$$

where $(\frac{\partial f}{\partial t})_{\text{coll}}$ represents the change of distribution function due to the electron scattering. In the steady-state and under application of a uniform electric field, the Boltzmann equation can be written as

$$\frac{e\mathbf{F}}{\hbar} \cdot \nabla_k f = \left(\frac{\partial f}{\partial t}\right)_{\text{coll}}. \tag{2}$$

Consider electrons in an isotropic, non-parabolic conduction band whose equilibrium Fermi distribution function is $f_0(k)$ in the absence of electric field. Note the

equilibrium distribution $f_0(k)$ is isotropic in $\mathbf{k}$ space but is perturbed when an electric field is applied. If the electric field is small, we can treat the change from the equilibrium distribution function as a perturbation which is first-order in the electric field. The distribution in the presence of a sufficiently small field can be written quite generally as

$$f(\mathbf{k}) = f_0(k) + f_1(k)\cos\theta\,, \tag{3}$$

where θ is the angle between $\mathbf{k}$ and $\mathbf{F}$ and $f_1(k)$ is an isotropic function of $\mathbf{k}$, which is proportional to the magnitude of the electric field. $f(\mathbf{k})$ satisfies the Boltzmann Eq. (2) and it follows that

$$\frac{eF\cos\theta}{\hbar}\frac{\partial f_0}{\partial k} = \sum_i \left\{ \int \cos\theta' f_1'[s_i'(1-f_0) + s_i f_0]d^3k' - f_1\cos\theta \int [s_i(1-f_0') + s_i' f_0']d^3k' \right\}, \tag{4}$$

where the sum is over scattering processes i. For a more compact notation, we have written $f(\mathbf{k}') = f'$, $s_i(\mathbf{k},\mathbf{k}') = s_i$ and $s_i(\mathbf{k}',\mathbf{k}) = s_i'$. $s_i(\mathbf{k},\mathbf{k}') = s_i$ is the probability for scattering out of state $\mathbf{k}$ into the differential element d^3k' at $\mathbf{k}'$. For the isotropic conduction band, $s_i(\mathbf{k},\mathbf{k}')$ depends on only $\mathbf{k}$, $\mathbf{k}'$ and the cosine of the angle ϕ between them, and the relation

$$\int \cos\theta' A(\cos\phi)d^3k' = \cos\theta \int \cos\phi A(\cos\phi)d^3k'\,, \tag{5}$$

may be used to manipulate Eq. (4). Here, $A(\cos\phi)$ is an arbitrary function of $\cos\phi$ but does not otherwise depend on θ and θ'. From Eqs. (4) and (5), we obtain

$$\frac{eF}{\hbar}\frac{\partial f_0}{\partial k} = \sum_i \left\{ \int \cos\phi f_1'[s_i'(1-f_0) + s_i f_0]d^3k' - f_1 \int [s_i(1-f_0') + s_i' f_0']d^3k' \right\}. \tag{6}$$

In general, there will be both elastic and inelastic scattering processes. For example, impurity scattering is elastic and acoustic and piezoelectric scattering are elastic to a good approximation at room temperature. However, polar and non-polar optical phonon scattering are inelastic. Labelling the elastic and inelastic scattering rates with subscripts *el* and *iel* respectively and recognising that, for any process i, $s_{eli}(\mathbf{k}',\mathbf{k}) = s_{eli}(\mathbf{k},\mathbf{k}')$, Eq. (6) can be written as

$$f_1(k) = \frac{(-eF/\hbar)(\partial f_0/\partial k) + \sum_j \int \cos\phi f_1'[s_{ielj}'(1-f_0) + s_{ielj} f_0]d^3k'}{\sum_i \int (1-\cos\phi)s_{eli}d^3k' + \sum_j \int [s_{ielj}(1-f_0') + s_{ielj}' f_0']d^3k'}\,. \tag{7}$$

Note the first term in the denominator is simply the momentum relaxation rate for elastic scattering. Equation (7) may be solved iteratively by the relation

$$f_{1n}(k) = \frac{(-eF/\hbar)(\partial f_0/\partial k) + \sum_j \int \cos\phi f_{1(n-1)}'[s_{ielj}'(1-f_0) + s_{ielj} f_0]d^3k'}{\sum_i \int (1-\cos\phi)s_{eli}d^3k' + \sum_j \int [s_{ielj}(1-f_0') + s_{ielj}' f_0']d^3k'}\,, \tag{8}$$

where $f_{1n}(k)$ is the perturbation to the distribution function after the nth iteration. It is interesting to note that if the initial distribution is chosen to be the equlibrium distribution, for which $f_1(k)$ is equal to zero, we get the relaxation time approximation result after the first iteration. We have found that convergence can normally be achieved after only a few iterations for small electric fields. Once $f_1(k)$ has been evaluated to the required accuracy, it is possible to calculate quantities such as the drift mobility μ, which is given by

$$\mu = \frac{\int \mathbf{v} \cdot \mathbf{F} f(\mathbf{k}) d^3k}{F^2 \int f(\mathbf{k}) d^3k} \,. \tag{9}$$

In terms of spherical coordinates,

$$\mu = \frac{\int_0^\infty v k^2 (f_1/F) dk}{3 \int_0^\infty k^2 f_0 dk} \,. \tag{10}$$

The Kane approximation relation[18] between electron group velocity and effective mass m^* in a non-parabolic band is

$$v(k) = \frac{\hbar k}{m^*} \frac{1}{(1 + 2\alpha E)} \,, \tag{11}$$

and substituting this result in Eq. (10), we find that

$$\mu = \frac{\hbar}{3m^* F} \frac{\int_0^\infty (k^3/1 + 2\alpha E) f_1 dk}{\int_0^\infty k^2 f_0 dk} \,. \tag{12}$$

Here, we have calculated low field drift mobility in GaN structures using the iterative technique. The effects of piezoelectric, acoustic deformation, polar optical phonons and ionized impurity scattering have been included in the model. It is also assumed that the electrons remain in the Γ-valley of the Brillouin zone. The valley is isotropic in the case of zincblende GaN and approximated as such for the wurtzite crystal structure.

3. Low-Field Transport Results in Bulk GaN

Low field electron mobility in GaN as a function of temperature and doping concentration has been performed by Dhar *et al.*[18] and Albercht *et al.*[19] Their calculations show that an electron mobility as high as 900 $\mathrm{cm^2 V^{-1} s^{-1}}$ could be achieved in the case of uncompensated GaN at room temperature. In the case of high quality samples with very low compensation, a mobility of more than 800 $\mathrm{cm^2 V^{-1} s^{-1}}$ at room temperature with a similar doping concentration has been reported. On the other hand, there has been very little work on the calculation of low-field electron mobility in GaN. Chin *et al.*[20] have used the variational principle to calculate low-field electron mobilities and compared their results with fairly old experimental data. They have tried to fit the experimental data with an overstimated compensation ratio. In old samples, low-field electron mobility was due to poor substrate and buffer

Table 1. Important parameters used in our calculations for zincblende and wurtzite GaN materials which are taken from Refs. 13–17.

	Zb-GaN	Wz-GaN
Density ρ (kgm^{-3})	6100	6150
Sound velocity v_s (ms^{-1})	4570	4330
Piezoelectric constant p (cm^{-2})	0.375	0.375
Longitudinal sound velocity v_s (ms^{-1})	4570	4330
Low-frequency dielectric constant ϵ_s	9.5	9.5
High-frequency dielectric constant ϵ_∞	5.35	5.35
Acoustic deformation potential D (eV)	8.3	8.3
Polar optical phonon energy $\hbar\omega_{op}$ (meV)	99	99
Bandgap E_g (meV)	3.2	3.5
Non-parabolicity α (eV^{-1})	0.213	0.189
Electron effective mass:		
$m^*_\parallel$ (Γ-A direction)	0.15	0.18
$m^*_\perp$ (Γ-M direction)	0.15	0.2

quality and other growth related problems. The iterative technique has been used by Rode and Gaskill[21] for low-field electron mobility in GaN for the dependence of mobility on electron concentration, but not on temperature, and ionized impurity scattering has been estimated within the Born approximation, which might be the reason for poor fitting at high electron concentrations.

Here, we have performed a series of low-field electron mobility calculations for both GaN structures. Low-field mobilities have been derived using iteration method. Important parameters used throughout the calculations are listed in Table 1. Figure 1 shows the calculated electron drift mobilities versus temperature and donor concentration for zincblende and wurtzite GaN. The electron drift mobilities at room temperature that we find are 1300 and 900 cm^{2}V^{-1}s^{-1} for zincblende and wurtzite structures, respectively, for an electric field equal to 10^4 Vm^{-1} and with a donor concentration of 10^{22} m^{-3}. The material parameters used to calculate the electron drift mobilities are tabulated in Table 1. For the wurtzite crystal structure, it is assumed that the conduction band is isotropic with an effective mass 0.2 m_0. This is a reasonable approximation since m^*_l and m^*_t differ by only 10%.

The results plotted in Fig. 1(a) indicate that the electron drift mobility of wurtzite GaN is lower than that for the zincblende structure at all temperatures. This is largely due to the higher Γ valley effective mass in the wurtzite phase. Figure 1(b) shows the calculated variation of the electron mobility as a function of the donor concentration for both GaN crystal structures at room temperature. The mobility does not vary monotonically between donor concentrations of 10^{21} and 10^{25} m^{-3} due to the dependence of electron scattering on donor concentration, but reaches a value of 1500 and 1000 cm^{2}V^{-1}s^{-1} for zincblende and wurtzite crystal structures, respectively. In order to understand the scattering mechanisms which limit the mobility of GaN under various conditions, we have performed calculations

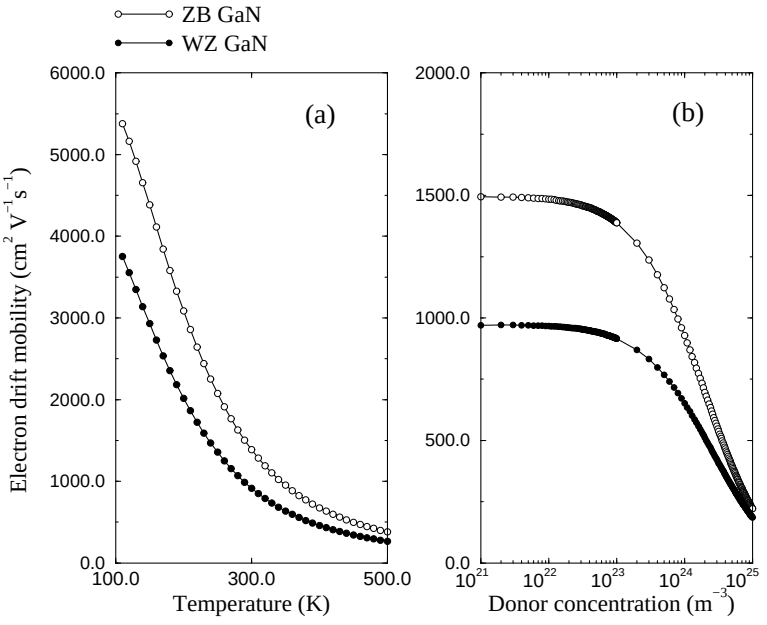

Fig. 1. (a) Electron drift mobility of GaN in zincblende and wurtzite structures versus temperature. Donor concentration is approximately 10^{22} m^{-3}. (b) Electron drift mobility of GaN in zincblende and wurtzite structures versus donor concentration at room temperature.

of the electron drift mobility when particular scattering processes are ignored. The solid curve in Fig. 2 shows the calculated mobility for wurtzite GaN including all scattering mechanisms whereas the dashed, dotted, and open-circle curves show the calculated mobility without ionized impurity, piezoelectric and polar optical scattering, respectively. It can be seen that below 300 K, the ionized impurity scattering is dominant while at the higher temperatures, electron scattering is predominantly by optical modes. Thus, the marked reduction in mobility at low temperatures seen in Fig. 2 can be ascribed to impurity scattering and that at high temperatures to polar optical phonon scattering. In Fig. 2, the mobility in the absence of band non-parabolicity is plotted as a dash-dot curve. Non-parabolicity leads to approximately a 10% reduction relative to the mobility for parabolic band at room temperature. This is because non-parabolicity increases the electron effective mass and also the scattering rates through the density of states.

The temperature variation of the electron drift mobility in zincblende and wurtzite GaN for different donor concentrations is shown in Fig. 3. It is evident from this figure that the curves approach each other at very high temperatures, where the mobility is limited by longitudinal optical phonon scattering, whereas the mobility varies inversely with donor concentration at low temperatures as we would expect from the foregoing discussion.

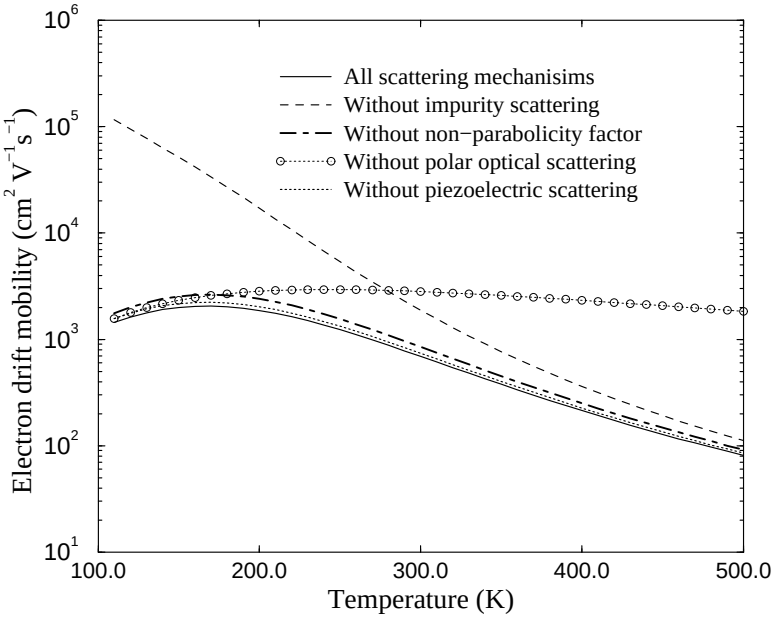

Fig. 2. Comparison of electron drift mobility in wurtzite GaN with donor concentration of 10^{24} m^{-3} and when individual scattering processes are ignored. The effect of Γ-valley non-parabolicity is also shown.

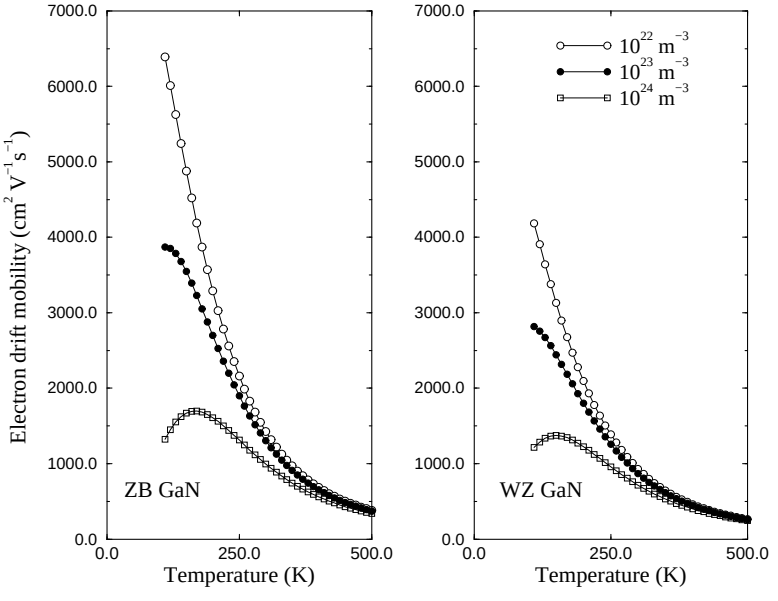

Fig. 3. Calculated low-field electron drift mobility of zincblende and wurtzite GaN as functions of temperature for different donor concentrations.

4. Conclusion

In conclusion, we have studied the electron transport characteristic associated with zincblende and wurtzite GaN. Temperature-dependent and free-electron concentration dependent of the electron mobility in both GaN structures have been compared. It has been found that the low-field electron mobility is significantly higher for the zincblende GaN structure than zincblende structure due to the lower Γ electron effective mass in this crystal structure. Several scattering mechanisms have been included in the calculation. Ionized impurities have been treated beyond the Born approximation using a phase shift analysis. Screening of ionized impurities has been treated more realistically using a multi-ion screening formalism, which is more relevant in the case of highly compensated III–V semiconductors like GaN.

Acknowledgment

This work benefitted from useful discussions with G. Crow and R. R. Abram.

References

1. S. Strite and H. Morkoc, *J. Vac. Sci. Technol. B* **10** (1992) 1237.
2. H. Morkoc, S. Strite, G. B. Gao and M. Burns, *J. Appl. Phys.* **76** (1994) 1363.
3. S. N. Mohammad and H. Morkoc, *Prog. Quant. Electron.* **20** (1996) 361.
4. S. J. Pearton, J. C. Zopler, R. J. Shul and F. Ren, *J. Appl. Phys.* **86** (1999) 1.
5. S. Nakamura, *Mater. Res. Soc. Bull.* **22** (1997) 29.
6. M. S. Shur and M. A. Khan, *Mater. Res. Soc. Bull.* **22** (1997) 44.
7. B. Gelmont, K. Kim and M. Shur, *J. Appl. Phys.* **74** (1993) 1818.
8. H. Morkoc, *Nitride Semiconductor and Devices* (Springer-Verlag, 1999).
9. R. P. Wang, P. P. Ruden, J. Kolnik and K. F. Brennan, *Mat. Res. Soc. Symp. Proc.* **445** (1997) 935.
10. C. Moglestue, *Monte Carlo Simulation of Semiconductor Devices* (Chapman and Hall, 1993).
11. B. K. Ridley, *Electrons and Phonons in Semiconductor Multilayers* (Cambridge University Press, 1997).
12. C. Jacoboni and P. Lugli, *The Monte Carlo Method for Semiconductor and Device Simulation* (Springer-Verlag, 1989).
13. D. L. Rode, *Phys. Rev. B* **2** (1970) 1012.
14. D. L. Rode, *Phys. Rev. B* **3** (1971) 3287.
15. D. L. Rode and A. C. Beer, *Phys. Rev. B* **3** (1971) 2534.
16. J. Kolnik, I. H. Oguzman and K. F. Brennan, *J. Appl. Phys.* **78** (1995) 1033.
17. B. E. Foutz, L. F. Eastman, U. V. Bhapkar and M. Shur, *Appl. Phys. Lett.* **70** (1997) 2849.
18. S. Dhar and S. Ghosh, *J. Appl. Phys.* **86** (1999) 2668.
19. J. D. Albrecht, R. P. Wang, P. P. Ruden and K. F. Brennan, *J. Appl. Phys.* **83** (1998) 2185.
20. V. W. Chin, T. L. Tansley and T. Osotchan, *J. Appl. Phys.* **75** (1994) 7365.
21. D. L. Rode and D. K. Gaskill, *Appl. Phys. Lett.* **66** (1995) 1972.